

Gaseous versus Stellar Velocity Dispersion in Emission-Line Galaxies*

Xiao-Yan Chen^{1,2,3}, Cai-Na Hao^{1,4} and Jing Wang²

¹ Tianjin Astrophysics Center, Tianjin Normal University, Tianjin 300384; chenxy@bao.ac.cn

² National Astronomical Observatories, Chinese Academy of Sciences, Beijing 100012

³ Graduate School of Chinese Academy of Sciences, Beijing 100049

⁴ Institute of Astronomy, Madingley Road, Cambridge CB3 0HA, UK

Received 2007 April 18; accepted 2007 May 12

Abstract We compare the ionized gas velocity dispersion σ_{gas} with the stellar velocity dispersion σ_* in star-forming galaxies, composite galaxies, Low Ionization Nuclear Emission-line Regions (LINERs) and Seyfert 2s, compiled from a cross-identification of Sloan Digital Sky Survey Fourth Data Release (SDSS DR4) and Point Source Catalogue Redshift Survey (PSCz). We measure σ_{gas} from the FWHMs of emission lines ($\text{H}\alpha$, $[\text{NII}]\lambda\lambda 6548, 6583$ and $[\text{SII}]\lambda\lambda 6716, 6731$). A significant correlation between the gas and stellar velocity dispersion exists, despite substantial scatter. The mean value of the gas to stellar velocity dispersion ratio is close to unity. This suggests that gas velocity dispersion can substitute for the stellar velocity dispersion as a tracer of the gravitational potential well for all the four types of galaxies, but the involved uncertainties are different from type to type. We also studied $\bar{\sigma}_{\text{gas}}/\sigma_*$ as a function of the redshift and the axial ratio to test the effects of aperture and galaxy inclination, and found that both effects are weak. Finally we checked the trend of $\bar{\sigma}_{\text{gas}}/\sigma_*$ with the infrared luminosity and found no significant correlation.

Key words: galaxies: active — galaxies: interactions — galaxies: star-forming — galaxies: Seyfert

1 INTRODUCTION

The dynamical mass of a galaxy is one of the most important properties of galaxies, and its estimation suffers from several uncertainties. Under the assumption that the system is in dynamical equilibrium, we can estimate it from an assumed model of mass distribution when we know its stellar velocity dispersion and size (Hinz & Rieke 2006). Leaving aside the size and the model of mass distribution, we will in this paper concentrate on the velocity dispersion. Now, it is generally more difficult to measure stellar velocity dispersion than the dispersion of the emission lines, so many studies use the velocity dispersion of the ionized gas as a substitute for the stellar velocity dispersion when estimating the dynamical mass of high-redshift star-forming galaxies (e.g., Pettini et al. 1998, 2001; Erb et al. 2003, 2006). However, it is then not clear to what extent the ionized gas velocity dispersion traces the gravitational potential.

There have been some studies on the relationship between the gas and stellar velocity dispersions in AGNs (e.g., Smith et al. 1990; Nelson & Whittle 1996; Nelson 2000, Zhang et al. 2002; Onken et al. 2004; Bonning et al. 2005; Botte et al. 2005; Lu et al. 2005; Bian et al. 2006; Gu et al. 2006; Liu et al. 2006). These authors have found that the gas kinematics of the narrow-line region of active galaxies are primarily governed by the gravitational potential of the stars, but to our knowledge, proper statistics has not been done on any large sample of star-forming galaxies.

* Supported by the National Natural Science Foundation of China.

Colina et al. (2005) studied the kinematic properties of the gas and star components of 11 nuclei of local ultraluminous infrared galaxies (ULIRGs). They found that there is a tight correlation between the velocity dispersions of the central ionized gas and the stars, with a ratio between the two of 1.01 ± 0.13 . The authors pointed out that this correlation justifies the use of the ionized gas velocity dispersion as a tracer of the dynamical mass for high-redshift star-forming galaxies, but they also noted some caveats, as the distribution of the ionized gas is often decoupled from that of the stars. As a result, they suggested that, to use the ionized gas velocity dispersion as a reliable tracer of the potential well, some a priori knowledge of the stellar light distribution traced by high spatial resolution optical or near-infrared imaging is required. However, it is difficult to obtain images with high angular resolution in the near- and mid-infrared for large samples; for example, there are just 114 star-forming galaxies in Erb et al. (2006). Although Colina et al. (2005) derived a tight correlation between the two dispersions, this correlation was based on only six points, with a majority of LINERs. Furthermore, the correlation may vary with the spectral type, infrared luminosity and inclination of the target galaxies. Therefore, it is necessary to investigate this correlation as a function of these other properties using a large sample.

In this study, we will examine the correlation between the ionized gas velocity dispersion and stellar velocity dispersion as a function of spectral type, redshift, inclination and infrared luminosity, using a large sample selected from cross-identification between SDSS DR4 and Infrared Astronomical Satellite (*IRAS*) PSCz. We can then estimate to what extent the potential well is traced by either velocity dispersions in different galaxy populations.

This paper is organized as follows. We present the sample selection and spectral classification in Section 2. Section 3 presents a detailed description of the methods we use to measure the velocity dispersions. We then present and discuss our results in Section 4. A summary is given in Section 5. Throughout this paper we assume the following cosmological parameters: matter density parameter $\Omega_m = 0.3$, cosmological constant $\Omega_\Lambda = 0.7$, and Hubble constant $H_0 = 70 \text{ km s}^{-1} \text{ Mpc}^{-1}$.

2 SAMPLE SELECTION AND SPECTRAL CLASSIFICATION

Our sample was selected from SDSS DR4. In order to investigate the relation of gas velocity dispersion versus stellar velocity dispersion ($\sigma_{\text{gas}} - \sigma_*$) as a function of the infrared luminosity, we restrict our sample to those with available *IRAS* observations. Specifically, we first selected all galaxies with redshifts less than 0.5 at confidence levels greater than 0.9 from SDSS DR4. Then these were cross identified with PSCz¹ objects using a $5''$ matching radius. To ensure reliability of the identifications, the optical positions of the PSCz objects were used. As the PSCz objects mostly have redshifts less than 0.1 (Saunders et al. 2000), the redshift distribution of our sample objects is almost truncated at redshift of 0.1 (see Fig. 1, left panel). We calculated the far-infrared luminosity L_{FIR} from the nominal flux densities, $f_\nu(60 \mu\text{m})$ and $f_\nu(100 \mu\text{m})$ in the *IRAS* catalogues (Helou et al. 1988; Sanders & Mirabel 1996) and the redshifts given by SDSS, and then converted it to the total infrared luminosity L_{IR} (1–1000 μm , Calzetti et al. 2000; Cao et al. 2006) according to the following formulae:

$$F_{\text{FIR}} = 1.26 \times 10^{-14} \{2.58 f_{60} + f_{100}\} [\text{W m}^{-2}], \quad (1)$$

$$L_{\text{FIR}} = 4\pi D_L^2 F_{\text{FIR}} [L_\odot], \quad (2)$$

$$L_{\text{IR}}(1 - 1000 \mu\text{m}) = 1.75 L_{\text{FIR}}. \quad (3)$$

SDSS DR4 includes over 800 000 fiber spectra of objects based on from the five-band (u, g, r, i and z) imaging (Fukugita et al. 1996; Smith et al. 2002; Strauss et al. 2002). Each fiber is $3''$ in diameter (Bernardi et al. 2003; Greene et al. 2005, 2006; Adelman-McCarthy et al. 2006), corresponding to $\sim 1.8 \text{ kpc}$ at $z = 0.03$ (the median redshift of our sample, see below and Fig. 1). The observed-frame spectral wavelength range is 3800–9200 \AA . The instrumental resolution of the spectra is $\lambda/\Delta\lambda \approx 1800$, equivalent to a Gaussian $\sigma_{\text{inst}} \approx 70 \text{ km s}^{-1}$ (Heckman et al. 2004; Greene et al. 2005, 2006).

¹ The *IRAS* PSCz survey is a redshift survey of about 15 000 galaxies detected in the *IRAS* Point Source Catalogue, after supplements and corrections (Saunders et al. 2000), containing 18 351 objects with $f_{60} > 0.6 \text{ Jy}$, covering 84% of the full sky, making it the largest ‘full-sky’ galaxy survey in existence.

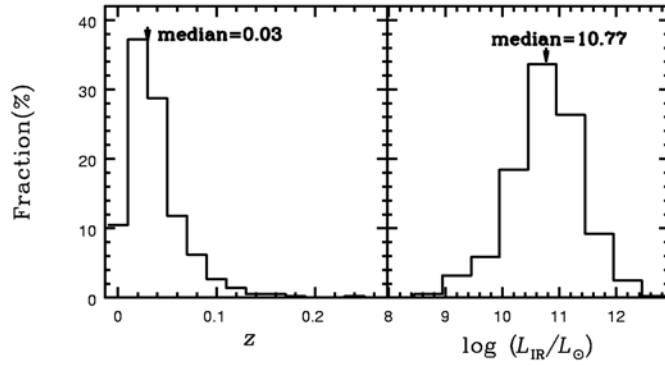


Fig. 1 Distribution of redshift (left) and infrared luminosity (right) for our sample of 913 objects.

The cross-identification yielded 1097 objects. In this work we use the stellar velocity dispersion values provided by MPA ² (Tremonti et al. 2004). There are 34 objects without stellar velocity dispersion measurements in the MPA catalogues and they are excluded from our sample. Furthermore, we excluded 15 objects with negative errors in σ_* and eight objects with extremely small (far less than 1) values of σ_* . So there are 1040 objects left.

To improve the accuracy of the measurements of the gas velocity dispersion, we further excluded 78 objects either with low emission-line signal-to-noise ratios (S/N) ($S/N < 5$ in $H\beta$, $H\alpha$, $[\text{NII}]\lambda 6583$, $[\text{SII}]\lambda\lambda 6716, 6731$, $S/N < 3$ in $[\text{OIII}]\lambda 5007$ line), or are badly fitted. To use different S/N cutoffs is because $[\text{OIII}]\lambda 5007$ is the faintest among the four lines. After the cutoff, 962 sources are left.

To ensure the spectra were taken at the centers of the galaxies (within a radius of 2'' from the center), we examine the positions of the fibers for all the sample objects. We found that there are 49 galaxies where the fiber is not located at the center. After discarding these, we are left with a total of 913 objects.

We classify the 913 sources as star-forming galaxies, composite galaxies, LINERs and Seyfert 2s according to the emission-line flux ratio diagnostic diagram (Eqs. (4) ~ (6), Baldwin et al. 1981; Veilleux & Osterbrock 1987; Kauffmann et al. 2003). First, we separated the star-forming galaxies, composite galaxies and AGNs by Equations (4) and (5) (Kewley et al. 2001; Kauffmann et al. 2003; Brinchmann et al. 2004). Then we divided the AGNs into LINERs and Seyfert 2s by Equation (6) (Shuder et al. 1981). The fluxes of these emission lines were derived from the MPA catalogues. We finally have 463 star-forming galaxies, 347 composite galaxies, 67 LINERs and 36 Seyfert 2s (column (2) of Table 1).

$$\log\left(\frac{[\text{OIII}]\lambda 5007}{H\beta}\right) = \frac{0.61}{\log([\text{NII}]\lambda 6583/H\alpha) - 0.47} + 1.19, \quad (4)$$

$$\log\left(\frac{[\text{OIII}]\lambda 5007}{H\beta}\right) = \frac{0.61}{\log([\text{NII}]\lambda 6583/H\alpha) - 0.05} + 1.3, \quad (5)$$

$$[\text{OIII}]\lambda 5007/H\beta = 3. \quad (6)$$

The redshifts of our sample range from 0.002 to 0.24, with a median of 0.03 (Fig. 1, left panel). Most of the targets (77%) have $z < 0.05$. The infrared luminosity spans a range of $\log(L_{\text{IR}}/L_{\odot}) = 8.65 - 12.48$, with a median of 10.77 (Fig. 1, right panel).

3 DATA ANALYSIS

In this section we discuss the data reduction and describe how we obtain the gas velocity dispersion from the emission lines. We downloaded the spectra in the one-dimensional FITS format ³ which have been sky subtracted, telluric absorption bands removed, and wavelength and spectrophotometry calibrated (Stoughton

² See http://www.mpa-garching.mpg.de/SDSS/DR4/raw_data.html.

³ <http://das.sdss.org/DR4/cgi-bin/DAS>

Table 1 Subsamples

Sample	Full	$\sigma_*/\sigma_{*error} < 5$	H α	$\left(\frac{FWHM}{FWHM_{error}}\right) < 5$		
				[NII]	[SII] λ 6716	[SII] λ 6731
	N	N	N	N	N	N
total	913	53	0	0	13	22
star-forming	463	44	0	0	2	2
composite	347	9	0	0	8	13
LINER	67	0	0	0	2	5
Seyfert2	36	0	0	0	1	2

et al. 2002). We corrected the Galactic extinction using the value from NED⁴ (Schlegel et al. 1998), then shifted the spectrum to the rest frame.

3.1 Starlight Subtraction

The spectra from SDSS are taken through a 3'' diameter fiber, which is large enough to include the light from the nucleus and some star light from the host galaxy. Absorptions can mask or weaken the emissions, and the continuum may also affect the measurement of the emission-line intensities. To obtain reliable widths of the emission-lines, the underlying stellar continuum is first removed.

The basic consideration of subtraction of the stellar components is to build a library of stellar absorption-line spectra templates, by applying the principal component analysis (PCA) technique (Li et al. 2005; Hao et al. 2005) to simple stellar population (SSP) models (Bruzual & Charlot 2003). We used a linear combination of the first seven eigenspectra, and a Galactic extinction curve (Cardelli et al. 1989) to model the stellar components (Wang et al. 2006). A χ^2 minimization was used over the region free of emission lines (3700 to 6800 Å) to acquire the best fit solution. Finally, the modeled spectrum was removed from the rest-frame spectrum obtained above. Figure 2 shows one case each of the starlight subtraction for the four galaxy types.

3.2 Emission Line Measurements

For each galaxy we measure five emission lines (H α , [NII] $\lambda\lambda$ 6583, 6548, [SII] $\lambda\lambda$ 6716, 6731). Their FWHMs were derived by fitting Gaussian profiles to the emission lines interactively, using the task SPECFIT (Kriss 1994) in the IRAF-STSDAS package⁵.

There is a strong correlation between the width of emission-line and the critical density (Filippenko et al. 1984; Sarzi et al. 2006), so different emission lines from the same atom may have different widths. De Robertis (1986) and Osterbrock (1989) measured some critical densities of narrow emission lines for some Seyfert 2s. They found that the [SII] $\lambda\lambda$ 6716, 6731 lines possess different critical densities, while the [NII] $\lambda\lambda$ 6548, 6583 doublets have the same critical density. Accordingly, for the [SII] $\lambda\lambda$ 6716, 6731 lines, we used two Gaussian profiles with independent FWHMs and intensities, while tying their central wavelengths together by their laboratory values. The H α and [NII] $\lambda\lambda$ 6548, 6583 lines are modeled using three Gaussians. The FWHMs of the [NII] $\lambda\lambda$ 6548, 6583 lines are kept the same, and the intensity ratio of [NII] λ 6583 to [NII] λ 6548 is fixed at 3:1, as required by the energy level structure of the [NII] ion (Osterbrock 1989). Again, their wavelengths are tied together and to H α by their laboratory values. We use these models to fit the five lines simultaneously and obtained four independent FWHMs.

We obtain the errors of our Gaussian fitting from SPECFIT, and list the median values of relative errors in Table 2. Examples of the Gaussian fitting are also presented in Figure 3 for the four galaxy types.

3.3 Calculating Velocity Dispersion

Assuming the emission-line profile to be Gaussian, as justified by the good fit, we compute the observed gas velocity dispersion from the FWHM of each emission line, with $\sigma'_{\text{g}} = \text{FWHM}/2.35$.

The observed line width is the convolution of the intrinsic line width and the instrumental resolution, so we obtain the intrinsic velocity dispersion by subtracting the latter σ_{inst} in quadrature and take into

⁴ NASA Extra-galactic Database

⁵ see details in <http://iraf.noao.edu/>

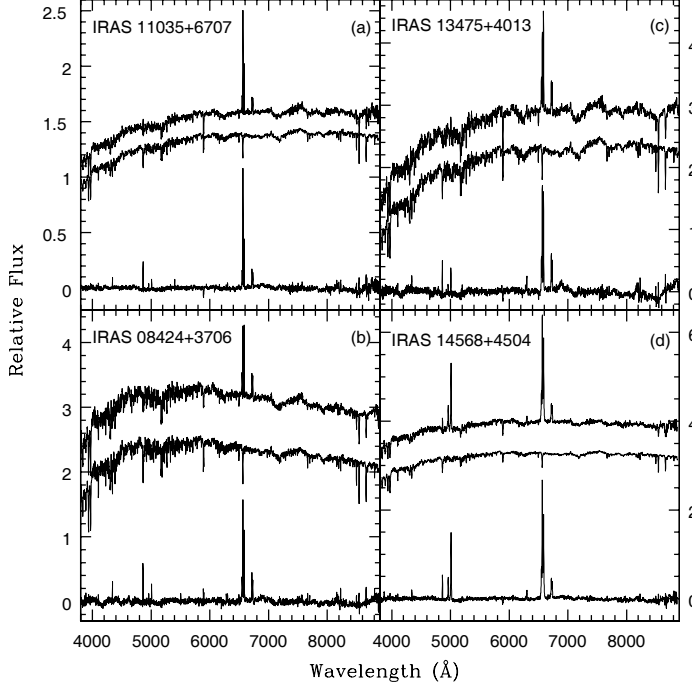


Fig. 2 Examples of starlight subtraction for a star-forming galaxy (a), a composite galaxy (b), a LINER (c) and a Seyfert 2 (d). In each panel, the observed spectrum, the best-fitting spectrum and the starlight-subtracted spectrum are shown from top to bottom, with a small offset for clarity.

Table 2 Median Values of Relative Errors in the Gaussian Fit of Each Emission Line

Sample	H α	[NII]	[SII] λ 6716	[SII] λ 6731
star-forming	0.5%	1.2%	3.0%	3.9%
composite	1.0%	1.6%	5.4%	6.7%
LINER	1.7%	2.0%	7.4%	9.4%
Seyfert 2	1.4%	1.8%	7.1%	8.9%

Notes— col: (1) sample.

cols: (2)–(5) median values of relative errors in Gaussian fitting for each emission-line.

account the redshift effect. The stellar velocity dispersions we obtained from the catalogue of MPA have already been corrected for the instrumental broadening effect. So we only need to correct the gas velocity dispersions.

We adopt a wavelength dependent instrumental resolution rather than a constant one. The instrumental resolutions at the line centers σ_{inst}^c (measured for each spectrum from the ARC lamps) are from the MPA catalogue. The intrinsic gas velocity dispersion σ_g is then computed using the following formula (z is the redshift):

$$\sigma_g = \sqrt{\left(\frac{\text{FWHM}}{2.35}\right)^2 - \left(\frac{\sigma_{\text{inst}}^c}{1+z}\right)^2}. \quad (7)$$

We list the median values of the relative errors in the gas velocity dispersions in Table 3. The errors of σ_{gas} are derived from the propagation of the errors of FWHM and z . Since the errors of z are very small, with a median value of 0.3% for star-forming galaxies, the error in the gas velocity dispersion mainly comes from the error in the FWHM. The line width measurements are also affected by the S/N of the emission

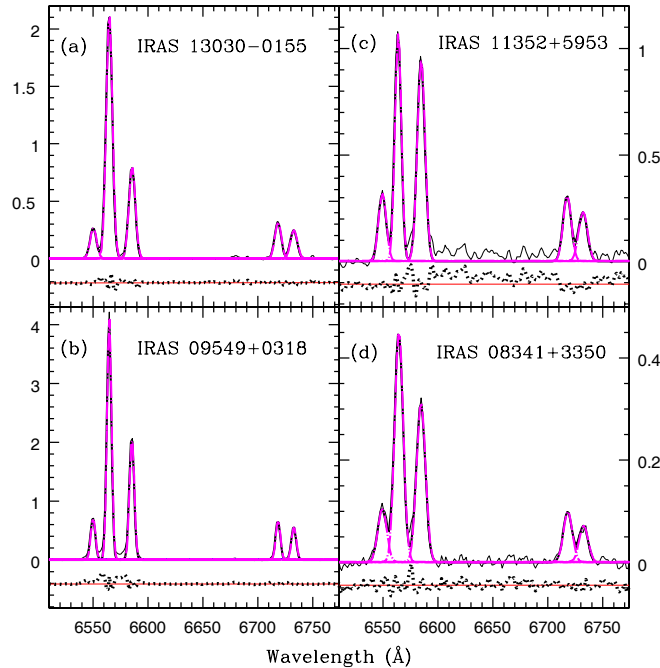


Fig. 3 Examples of Gaussian fitting for the four types of galaxies in the same sequence of panels as in Fig. 2. The solid lines represent the observed spectra, the short dashed lines the best-fitting profiles, the dot-long-dashed lines the best-fitting individual component, and the dotted lines are the residual spectra.

Table 3 Median Values of Relative Errors in Gas Velocity Dispersions for Each Emission Line

Sample	H α	[NII]	[SII] λ 6716	[SII] λ 6731
star-forming	0.7%	1.8%	4.6%	6.0%
composite	1.3%	2.0%	6.7%	8.2%
LINER	2.3%	2.5%	8.8%	11.3%
Seyfert 2	1.8%	2.2%	8.2%	8.9%

Notes— col: (1) sample. cols: (2)–(5) median values of relative errors in gas velocity dispersions for each emission-line.

lines, the uncertainty in the starlight subtraction and the line profiles, besides those mentioned in Kriss (1994). So the errors listed in Table 3 are probably underestimates.

4 RESULTS AND DISCUSSION

4.1 The $\sigma_{\text{gas}} \sim \sigma_*$ Relation

A comparison between the gas and stellar velocity dispersions for the four subsamples (star-forming galaxies, composite galaxies, LINERs and Seyfert 2s) is presented in Figures 4–7. Different symbols represent different types of sources, as indicated in Table 1. We can see that there is a significant correlation between the two velocity dispersions, despite substantial scatter. A vast majority of the sources lie within the bounds $\log(\sigma_{\text{gas}}/\sigma_*) = \pm 2$, and most of them are actually close to the diagonal $\sigma_{\text{gas}} = \sigma_*$.

Still, there are some outliers in these figures. To examine more closely these outliers with dramatically different gas and stellar velocity dispersions, we pick out those outside of the lines $\log(\sigma_{\text{gas}}/\sigma_*) = \pm 2$, and examine their other properties, such as the axial ratio (derived from SDSS DR5), redshift, morphology and spectrum.

There are 12 objects with $\sigma_{\text{gas}}/\sigma_* > 2$ in Figure 4. Most of these have $\sigma_*/\sigma_{*\text{error}} < 5$, of the exceptions, two have asymmetrical spiral arms, one has a small image and one is a normal object (i.e., the image

Table 4 Mean Values of $\sigma_{\text{gas}}/\sigma_*$ for Each Emission Line in Different Subsamples

Sample	H α	[NII]	[SII] λ 6716	[SII] λ 6731
star-forming	0.95 ± 0.16	0.96 ± 0.16	0.99 ± 0.18	1.01 ± 0.2
composite	0.95 ± 0.12	1.02 ± 0.15	1.04 ± 0.19	1.06 ± 0.2
LINER	0.94 ± 0.06	1.1 ± 0.07	1.16 ± 0.13	1.2 ± 0.17
Seyfert 2	1.07 ± 0.07	1.18 ± 0.08	1.06 ± 0.12	1.1 ± 0.13

Notes— Col: (1) sample. Cols: (2)–(5) mean values of $\sigma_{\text{gas}}/\sigma_*$ with errors (mean values) in each emission line for different subsamples.

is not too small and the spectrum is not badly fitted). We presume that most of the objects lying outside the line $\sigma_{\text{gas}}/\sigma_* > 2$ are those with large uncertainties in the possibly underestimated values of σ_* . We also examined the 12 objects with $\sigma_{\text{gas}}/\sigma_* < 0.5$. We find that the most dramatic outlier is one with a relatively high redshift ($z = 0.13$), a very small angular size, with almost the entire galaxy included in the fiber. Then there are three other objects with small sizes, the fibers covering about 25% to 50% of the galaxy. The remainder consists of four interacting galaxies: one compact galaxy and three normal galaxies (the same meaning as above).

In Figure 5, there are six objects with $\sigma_{\text{gas}}/\sigma_* > 2$. Four of them are objects with large errors in σ_* while the other two have no peculiar properties. Also, 19 objects have $\sigma_{\text{gas}}/\sigma_* < 0.5$, half of which are relatively high z ($z \geq 0.05$) galaxies with small angular sizes, having 20% to 100% of the entire galaxy included in the fiber. As regards morphology, at least seven of the outliers show evidence of interacting or irregular features, while at least five are normal.

In Figure 6, there are two objects with $\sigma_{\text{gas}}/\sigma_* < 0.5$, both of which are relatively high z objects ($z \geq 0.06$) with small sizes, and 50% to 100% of the galaxy are contained in the fiber. There are two objects with $\sigma_{\text{gas}}/\sigma_* > 2$, one is a normal galaxy, the other is an interacting galaxy. In Figure 7, there is one object with $\sigma_{\text{gas}}/\sigma_* > 2$. It has asymmetrical spiral arms.

In summary, large uncertainties in σ_* are mainly responsible for the large values of $\sigma_{\text{gas}}/\sigma_*$. On the other hand, we do not find any common properties among the objects with small values of $\sigma_{\text{gas}}/\sigma_*$: There may be several, equally important contributing factors here. Many of these objects are actually objects at higher redshifts ($z \geq 0.05$ or so), where large fractions of the entire galaxy are included within the fiber, implying greater contamination from the disk. Also, many of them are interacting galaxies, which may also affect the estimated velocity dispersions.

We calculated the mean values of $\sigma_{\text{gas}}/\sigma_*$ for each subsample. See Table 4. We can see that the gas velocity dispersion estimated using all four emission lines is as good as the stellar velocity dispersion for tracking the galactic potential well within the errors of the subsamples, although they give slightly different results. The mean values of $\sigma_{\text{gas}}/\sigma_*$ for the four emission lines are all approximately equal to 1.0 for the star-forming galaxies and composite galaxies. This suggests that the kinematics of both the stars and the gas are dominated by the same gravitational potential in the star-forming and composite galaxies. For LINERs and Seyfert 2s, the gas velocity dispersions estimated from the forbidden lines appear to be a little larger than the stellar velocity dispersions on average. This may suggest the existence of some other line broadening mechanisms in these two types, such as outflow, as shown by the blueshifts of these lines in many of such targets. However, within the errors they agree with each other well enough. This indicates that gravitational potential plays an important role in dominating the gas motion, while other secondary mechanisms are not so important. Colina et al. (2005) measured H α velocity dispersion, and obtained, for six nuclei of five sources (3 LINERs, 1 HII, 1 S2/LI), the statistical result $\langle \sigma_{\text{gas}}/\sigma_* \rangle = 1.01 \pm 0.13$, in agreement with our results for LINERs. Greene & Ho (2005) studied the ratio $\sigma_{\text{gas}}/\sigma_*$ for a large sample of 1749 Seyfert 2s. They estimated the σ_{gas} using several narrow lines. There is only have one emission line [SII] $\lambda\lambda$ 6716, 6731⁶ in common with us, for which they obtained a dispersion ratio of 1.11 ± 0.35 , in good agreement with our results for the Seyfert 2s (see Table 4). These good agreements show that our results are statistically robust.

⁶ They used the same width for the doublets.

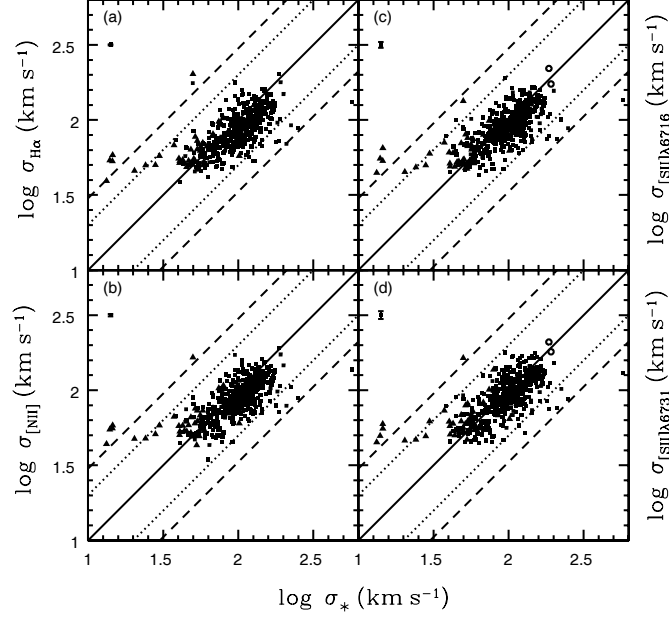


Fig. 4 A plot of σ_{gas} vs. σ_* (both in units of km s^{-1}) for star-forming galaxies. The filled triangles represent objects with $\sigma_*/\sigma_{*\text{error}} < 5$, filled squares represent objects with $\sigma_*/\sigma_{*\text{error}} > 5$ and $\frac{\text{FWHM}}{\text{FWHM}_{\text{error}}} > 5$, while open circles represent objects with $\frac{\text{FWHM}}{\text{FWHM}_{\text{error}}} < 5$. The solid line represents $\sigma_{\text{gas}}/\sigma_* = 1$, the dotted lines $\sigma_{\text{gas}}/\sigma_* = 2, 1/2$, and the dashed lines $\sigma_{\text{gas}}/\sigma_* = 3, 1/3$. The median errors are shown at the upper left corner.

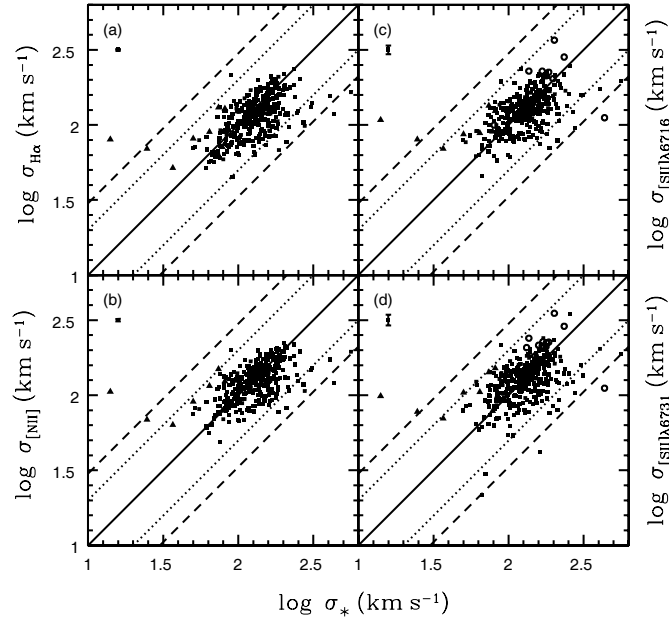


Fig. 5 A plot of σ_{gas} vs. σ_* (both in units of km s^{-1}) for composite galaxies. All the symbols have the same meaning as in Fig. 4.

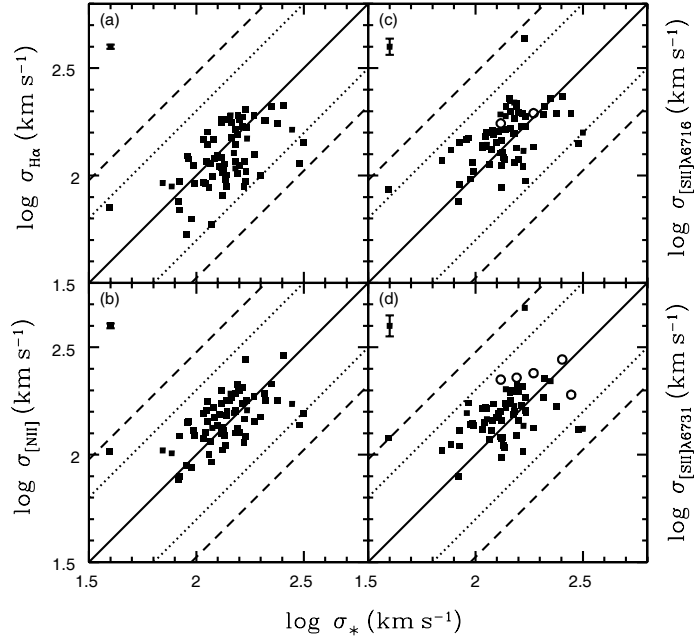


Fig. 6 A plot of σ_{gas} vs. σ_* (both in units of km s^{-1}) for LINERs. All the symbols have the same meanings as in Fig. 4.

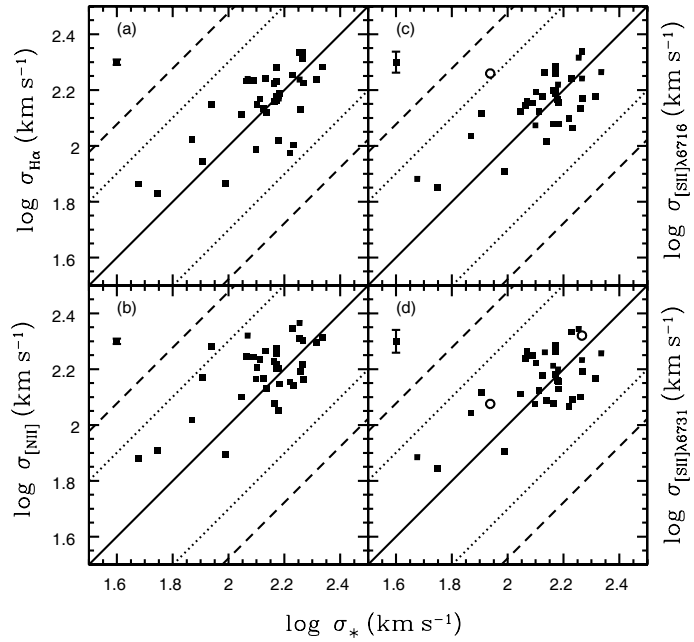


Fig. 7 A plot of σ_{gas} vs. σ_* (both in units of km s^{-1}) for Seyfert 2s. All the symbols have the same meaning as in Fig. 4.

4.2 $\sigma_{\text{gas}}/\sigma_*$ vs. Other Parameters

To avoid proliferation of figures, we adopt the weighted mean of the four emission line velocity dispersions as the characteristic gas velocity dispersion $\bar{\sigma}_g$. We shall simply use the inverse of the variance as the weight:

$$\bar{\sigma}_g = \left(\sum \frac{\sigma_g}{\sigma_{g\text{error}}^2} \right) / \left(\sum \frac{1}{\sigma_{g\text{error}}^2} \right), \quad (8)$$

$$\bar{\sigma}_{g\text{error}} = \sqrt{1 / \left(\sum \frac{1}{\sigma_{g\text{error}}^2} \right)}. \quad (9)$$

We examine whether the above correlation is affected by other properties. First, we study the $\bar{\sigma}_g/\sigma_*$ ratio as a function of the redshift. As the redshift range of our sample is small ($0 \sim 0.2$), there should not be an evolutionary effect. So this can be used as a test of the aperture effect. The SDSS spectra measure the light within a fixed aperture of radius $1''.5$, corresponding to 0.8 kpc at the median redshift of our sample ($z = 0.03$), to 1.5 kpc at $z = 0.05$, and to 5.7 kpc at the maximum redshift of our sample ($z = 0.24$). When a galaxy has a larger redshift, a larger fraction of the galaxy is included in the fiber. Therefore, the measured velocity dispersions for more distant galaxies are expected to be more affected by the radial variation of the velocity dispersion and the kinematics of the disk at larger physical radii. However, we cannot disentangle these two effects using the current data. Instead, we simply examine them together by plotting the $\bar{\sigma}_g/\sigma_*$ ratio versus the redshift. See Figure 8. The data points with error bars in panels (a) and (b) are the median values for galaxies in redshift bins of width 0.01 (the last bin has width, a larger in order to include all the

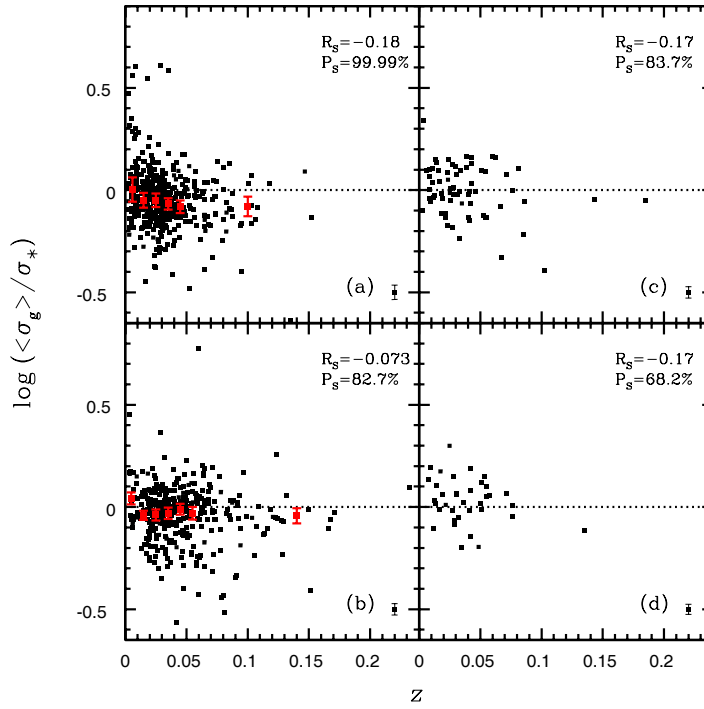


Fig. 8 Panels (a) to (d) show, respectively, the relation between $\bar{\sigma}_{\text{gas}}/\sigma_*$ and z for star-forming galaxies, composite galaxies, LINERs and Seyfert 2s. The data points with error bars in panels (a) and (b) are median values in bins of width 0.01 in z (except the last bin which has an appropriately larger width). The Spearman-Rank Order correlation coefficient and its significance are shown at the top right. The median error bars are shown at the bottom right corner.

remaining objects). We can see that there is a weak trend of $\bar{\sigma}_g/\sigma_*$ with z for the star-forming galaxies, but no trend for the composite galaxies. As for the AGNs, we cannot draw any firm conclusion because of the small sample size. So the aperture effect on our estimated velocity dispersion ratios can be taken as negligible (see Greene & Ho 2005 for a more detailed discussion).

The velocity dispersion measured from the emission lines are composed of a systematic, rotational component σ_{rot} (e.g., rotation), and a random component, σ_{ran} (e.g., random motion). For a disk with an inclination angle i and axial ratio $a/b = \cos i$, the observed velocity dispersion σ_o is: $\sigma_o^2 = (\sin i)^2 \sigma_{\text{rot}}^2 + \sigma_{\text{ran}}^2$ (Whittle 1985). As the distributions of stars and gas may be different, the rotational broadening may affect their observed velocity dispersion differentially. To investigate the effect of the differential rotational broadening effect on the estimated gas and stellar velocity dispersions, we examine how the dispersion ratio varies with the axial ratio. We obtain the axial ratios in the r-band from SDSS DR5 and an exponential profile fitting to the two-dimensional image. Figure 9 shows the plot of the $\bar{\sigma}_g/\sigma_*$ ratio versus the axial ratio a/b for each of the four subsamples, along with the Spearman-Rank Order correlation coefficient and its significance level. The data points with error bars in panels (a) and (b) are the median values for galaxies in bins of width 0.2 in axial ratio. The figure shows that there is a very weak trend of $\bar{\sigma}_g/\sigma_*$ with the axial ratio a/b for all the four subsamples, so the conclusion is that the differential rotational broadening effect is small.

Finally, we examine the correlation between $\bar{\sigma}_g/\sigma_*$ and the infrared luminosity in Figure 10, and perform the Spearman-Rank Order correlation analysis. The data points with error bars in Figure 10, panels (a) and (b) are the median values for galaxies in bins of width 0.5 in the infrared luminosity. We find that the

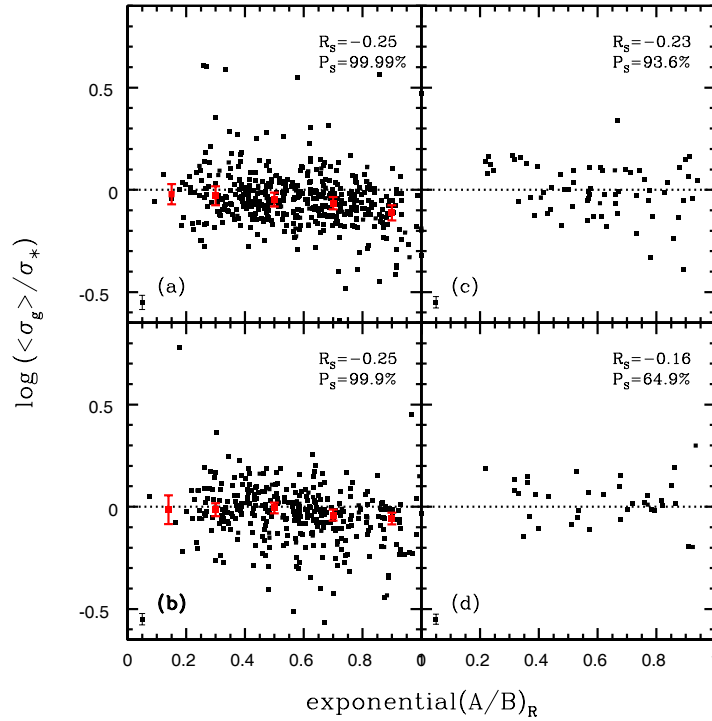


Fig. 9 Panels (a) to (d) show, respectively, the relation between the ratio $\bar{\sigma}_{\text{gas}}/\sigma_*$ and the axial ratio (exponential) for star-forming galaxies, composite galaxies, LINERs and Seyfert 2s. The data points with error bars in panels (a) and (b) are the median values for galaxies in bins of width 0.2 in axial ratio. The Spearman-Rank Order correlation coefficient and its significance are shown at the top right. The median error bars are shown at the bottom left corner.

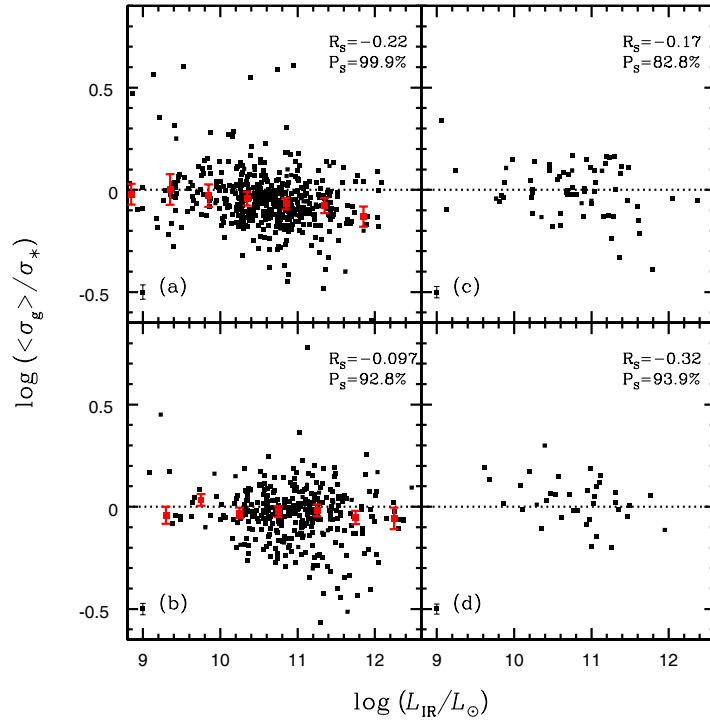


Fig. 10 Panels (a) to (d) show, respectively, the relation between $\overline{\sigma}_{\text{gas}}/\sigma_*$ and infrared luminosity L_{IR} for star-forming galaxies, composite galaxies, LINERs and Seyfert 2s. The data points with error bars in panels (a) and (b) are the median values for galaxies in bins of width 0.5 in the infrared luminosity. The Spearman-Rank Order correlation coefficient and its significance level are shown at the top right. The median error bars are shown at the bottom left corner.

trends of $\overline{\sigma}_g/\sigma_*$ with L_{IR} are similar to the trends of the ratio with z for the four subsamples. This indicates that for galaxy populations with different infrared luminosity, the ratio of gas velocity dispersion to stellar velocity dispersion does not vary systematically, although the morphology of the galaxies changes with L_{IR} (Sanders & Mirabel 1996). So the extrapolation of the relation derived from local ULIRGs to high-redshift Lyman-break galaxies (LBGs) and other UV selected galaxies by Colina et al. (2005) is probably reasonable.

We also tested all these three effects for each emission line separately, and obtained the same results as above, using the weighted mean gas velocity dispersion.

5 SUMMARY AND CONCLUSIONS

In this paper, based on a large sample of galaxies selected from a cross-identification of the SDSS DR4 and PSCz, we compared the stellar and gas velocity dispersions of the galaxies, the latter calculated from the FWHM of four emission lines, severally for star-forming galaxies, composite galaxies, LINERs and Seyfert 2s.

A significant correlation between the gas and stellar velocity dispersions is found, despite substantial scatter. From the statistics of the gas to stellar velocity dispersion ratio, we find that its mean value is close to 1 but the individual values are spread over a wide ranges. So we suggest that the gas velocity dispersion can substitute for the stellar velocity dispersion as a tracer of the galactic potential well for all the four types of galaxies, involving, however, different size uncertainties for galaxy populations of different spectral types.

Furthermore, we examined whether our conclusion is affected or related to other factors such as the spectral fiber aperture, disk rotational components, and infrared luminosities. It turns out that none of these effects are significant.

Acknowledgements We would like to thank professors Z. H. Shang, H. Wu, S. Mao, X. Y. Xia, Z. G. Deng for constructive suggestions. X. Y. Chen also thanks J. L. Wang, F. S. Liu, C. Cao, Y. N. Zhu for helpful discussions. We are grateful to David Schlegel for his explanation on the calculation of stellar velocity dispersion. We also thank an anonymous referee for his/her suggestions that improved the paper. C. N. Hao acknowledges the support from the Royal Society China Fellowship Programme. This work is supported by the NSFC Grants 10333060, 10778622, 10503005 and 10473013. This work has used the *IRAS* data from the PSCz, the spectra from SDSS DR4, and the emission line data from MPA. Funding for the SDSS and SDSS-II has been provided by the Alfred P. Sloan Foundation, the Participating Institutions, the National Science Foundation, the U.S. Department of Energy, the National Aeronautics and Space Administration, the Japanese Monbukagakusho, the Max Planck Society, and the Higher Education Funding Council for England. The SDSS is managed by the Astrophysical Research Consortium for the Participating Institutions. The Participating Institutions are the American Museum of Natural History, Astrophysical Institute Potsdam, University of Basel, Cambridge University, Case Western Reserve University, University of Chicago, Drexel University, Fermilab, the Institute for Advanced Study, the Japan Participation Group, Johns Hopkins University, the Joint Institute for Nuclear Astrophysics, the Kavli Institute for Particle Astrophysics and Cosmology, the Korean Scientist Group, the Chinese Academy of Sciences (LAMOST), Los Alamos National Laboratory, the Max-Planck-Institute for Astronomy (MPIA), the Max-Planck-Institute for Astrophysics (MPA), New Mexico State University, Ohio State University, University of Pittsburgh, University of Portsmouth, Princeton University, the Naval Observatory, and the University of Washington.

References

- Adelman-McCarthy J. K. et al., 2006, *ApJS*, 162, 38
Baldwin J. A., Phillips M. M., Terlevich R., 1981, *PASP*, 93, 5
Bernardi M. et al., 2003, *AJ*, 125, 1817
Bian W. et al., 2006, *MNRAS*, 372, 876
Bonning E. W. et al., 2005, *ApJ*, 626, 89
Botte V. et al., 2005, *MNRAS*, 356, 789
Brinchmann J. et al., 2004, *MNRAS*, 351, 1151
Bruzual G., Charlot S., 2003, *MNRAS*, 344, 1000
Calzetti D. et al., 2000, *ApJ*, 533, 682
Cao C. et al., 2006, *Chin. J. Astron. Astrophys. (ChJAA)*, 6, 197
Cardelli J. A., Clayton G. C., Mathis J. S., 1989, *ApJ*, 345, 245
Colina L., Arribas S., Monreal-Ibero A., 2005, *ApJ*, 621, 725
De Robertis M. M., Osterbrock D. E., 1986, *ApJ*, 301, 727
Erb D. K. et al., 2003, *ApJ*, 591, 101
Erb D. K. et al., 2006, *ApJ*, 646, 107
Filippenko A. V., Halpern J. P., 1984, *ApJ*, 285, 458
Fukugita M., Ichikawa T., Gunn J. E. et al., 1996, *AJ*, 111, 1748
Greene J. E., Ho L. C., 2005, *ApJ*, 627, 721
Greene J. E., Ho L. C., 2006, *ApJ*, 641, 117
Gu Q. et al., 2006, *MNRAS*, 366, 480
Hao L. et al., 2005, *AJ*, 129, 1783
Heckman T. M. et al., 2004, *ApJ*, 613, 109
Helou G., Khan I. R., Malek L. et al., 1988, *ApJS*, 68, 151
Hinz J. L., Rieke G. H., 2006, *ApJ*, 646, 872
Kauffmann G. et al., 2003, *MNRAS*, 346, 1055
Kewley L. J. et al., 2001, *ApJ*, 556, 121
Kriss G. A., 1994, *ASPC*, 61, 437

- Li C., Wang T.-G., Zhou H.-Y. et al., 2005, *AJ*, 129, 669
- Liu Y., Dong R.-J., astro-ph/0612260
- Lu H.-L., Zhou H.-Y., Wang T.-G. et al., 2005, *Chin. J. Astron. Astrophys. (ChJAA)*, 5, 221
- Nelson C. H., Whittle M., 1996, *ApJ*, 465, 96
- Nelson C. H., 2000, *ApJ*, 544, L91
- Onken C. A. et al., 2004, *AJ*, 615, 645
- Osterbrock, D. E., 1989, *Astrophysics of Gaseous Nebulae and Active Galactic Nuclei*, Mill Valley CA: University Science Books
- Pettini M., 1998, *ApJ*, 508, 539
- Pettini M., 2001, *ApJ*, 554, 981
- Sanders D. B., Mirabel I. F., 1996, *ARA&A*, 34, 749
- Sarzi M. et al., 2006, *MNRAS*, 366, 1151
- Saunders W. et al., 2000, *MNRAS*, 317, 55
- Schlegel D. J. et al., 1998, *ApJ*, 500, 525
- Shuder J. M., Osterbrock D. E., 1981, *ApJ*, 250, 55
- Smith E. P. et al., 1990, *ApJ*, 356, 399
- Smith J. A. et al., 2002, *AJ*, 123, 2121
- Stoughton C. et al., 2002, *AJ*, 123, 485
- Strauss M. A. et al., 2002, *AJ*, 124, 1810
- Tremonti C. A. et al., 2004, *ApJ*, 613, 898
- Veilleux S., Osterbrock D. E., 1987, *ApJS*, 63, 295
- Wang J., Wei J. Y., 2006, *ApJ*, 648, 158
- Whittle M., 1985, *MNRAS*, 213, 1
- Zhang T.-Z., Wu X.-B., 2002, *Chin. J. Astron. Astrophys. (ChJAA)*, 2, 487